CFD on Small Flow Injection of Advanced Accumulator in APWR

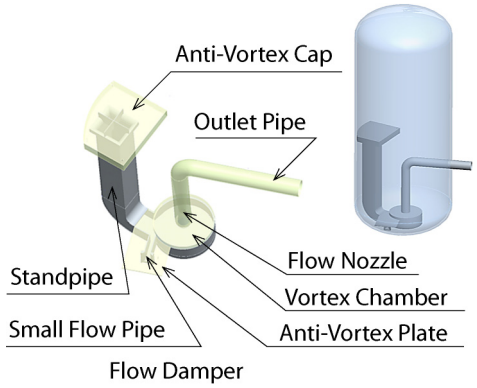

TOMOSHIGE TAKATA TAKAFUMI OGINO
TAKASHI ISHIBASHI TADASHI SHIRAISHI

The advanced accumulator in the advanced pressurized-water reactor is a system used to inject coolant into the reactor in the event of an emergency such as a loss-of-coolant accident, and can automatically change the injection flow rate from large to small using fluidics technology without moving parts. Its performance was demonstrated in a 1/2-scale injection test at the operating pressure. This paper describes the numerical analysis performed to investigate the generation mechanism of fluid resistance that reduces the flow rate in small flow injection. We show that the characteristics of the accumulator in small flow injection do not depend significantly on the scale of the test apparatus.

1. Introduction

We developed a flow damper using fluidics technology. We also developed an advanced accumulator injection system capable of two-stage switching of the injection flow rate using the developed flow damper to simplify and increase the reliability of the safety components of the emergency core cooling system of our advanced pressurized-water reactor (APWR) power plant[(1)]. The accumulator functions both as a conventional accumulator and a low-head injection system, and it can change the flow rate without using moving parts. We previously conducted a performance demonstration test that simulated the operating conditions in the event of an emergency using pressures including the accumulator operating pressure with 1/5- and 1/2-scale models. The test demonstrated the flow characteristics and operational reliability of the accumulator.

We also established a method for evaluating the performance of the advanced accumulator based on the scale-model test data, taking into account the test results. This paper reports the results of the numerical analysis of the flow in the flow damper during small flow injection.

2. Characteristics of the advanced accumulator

The advanced accumulator can automatically change the injection flow rate from a large one (performed by the accumulator in a conventional PWR) to a small one (performed by the low-pressure injection system in a conventional PWR) without any moving parts. The system relies on fluidics technology, a field in which flow is controlled using flow phenomena such as vortexes, wall-attaching flows, and collision of jets.

Because no moving parts are involved, the advanced accumulator has advantages such as a long service life, easy maintenance, and the ability to operate correctly in a severe environment. The construction and working principles of the accumulator are described below.

The accumulator has a flow damper consisting of a standpipe and a vortex chamber inside a tank. One of the two inlets (the large flow inlet) to the flow damper is located above the standpipe and the other one (the small flow inlet) is located below. When the water level in the tank is higher than the stand pipe inlet, as shown in **Figure 1**, the borated water flows from the two inlets merge in the vortex chamber and go straight out to the outlet pipe through the outlet port in the center. The borated water is injected at a large flow rate due to minimal flow resistance.

When the water level in the tank drops and the borated water supply through the stand pipe inlet stops, the water is supplied only through the small flow inlet. The borated water from the small flow inlet forms a strong vortex in the vortex chamber and flows out to the outlet pipe through the outlet port in the center. The kinetic energy of the swirling fluid is gradually dissipated as the fluid flows away from the center of the vortex chamber, generating large flow resistance and resulting in small flow injection.

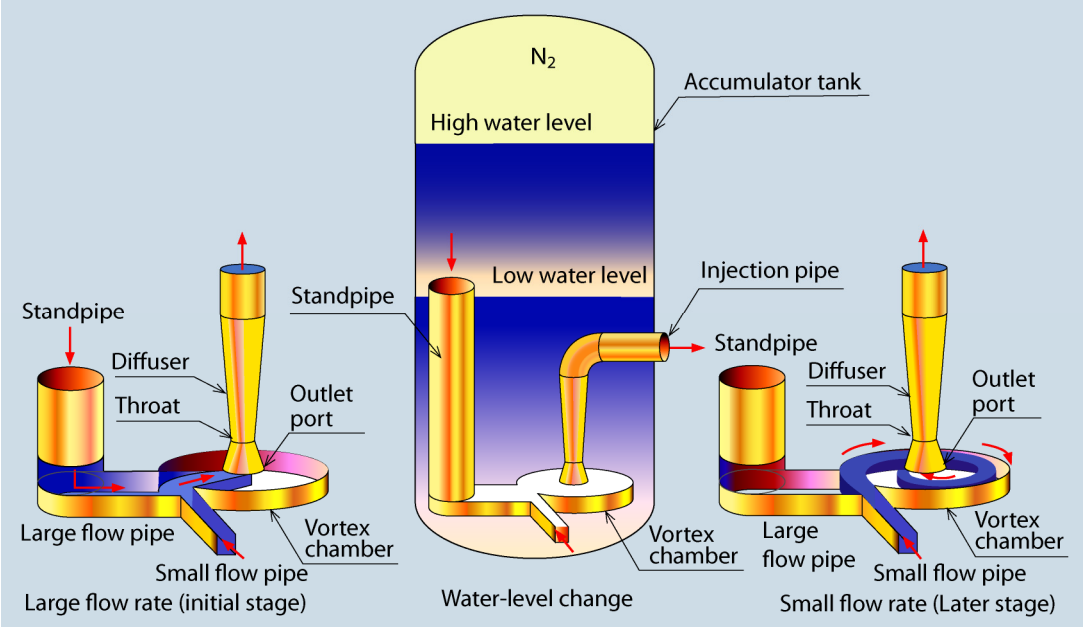

Figure 1 Flow rate control mechanism of the advanced accumulator
The flow rate can be automatically changed from large to small. When the fluid level is high, the fluid is injected smoothly at a large flow rate. When the fluid level is low, a vortex is formed and the fluid is injected at a small flow rate.

3. Analysis method

A computational fluid dynamics (CFD) analysis model to simulate the 1/5-, 1/2-, and full-scale flow dampers was developed to analyze the steady-state flow behavior in the section from the vortex chamber to the injection pipe downstream of the throat (**Figure 2**) during small flow injection. A hexahedral mesh was generated with a finer mesh for the region near the wall surface and the vortex core (i.e., the center of the vortex chamber) to capture the boundary layer and the vortex in high resolution. The number of mesh points was 3–4 million and nearly the same for the 1/5-, 1/2-, and full-scale analytical models.

In the analysis, cavitation numbers (σ) of 0.3 and 9.4 were used to cover the expected range of variation in the actual equipment during an accident. The cavitation number is calculated by $\sigma = (Pd - Pv)/\Delta P$, where Pd is the downstream static pressure, Pv is the vapor pressure, and ΔP is the pressure drop. Measured data from the 1/2-scale model test were used for the fluid temperature, inlet-plane velocity, and injection pipe outlet pressure.

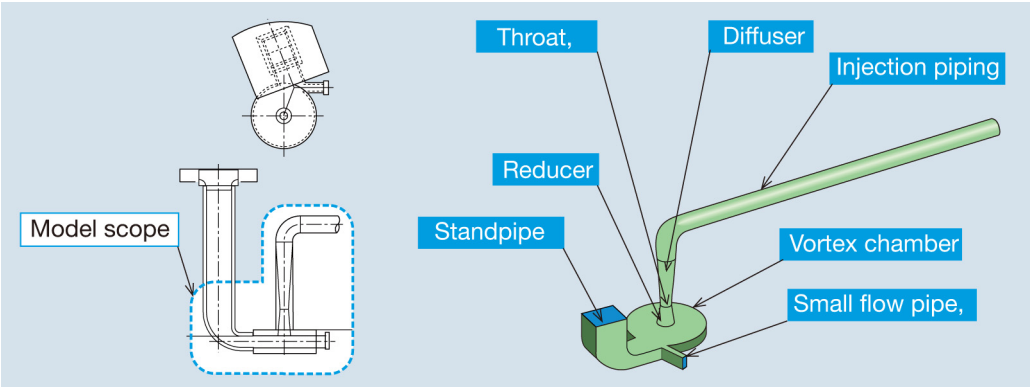

Figure 2 Schematic of the analysis model
The model covered the section from the small flow pipe inlet and the standpipe through the vortex chamber to the injection pipe downstream of the throat.

4. Analysis results

Figures 3–5 show the flow pattern, total pressure distribution, and turbulent energy distribution, respectively, in the scale model. From these figures, the following conclusions can be drawn.

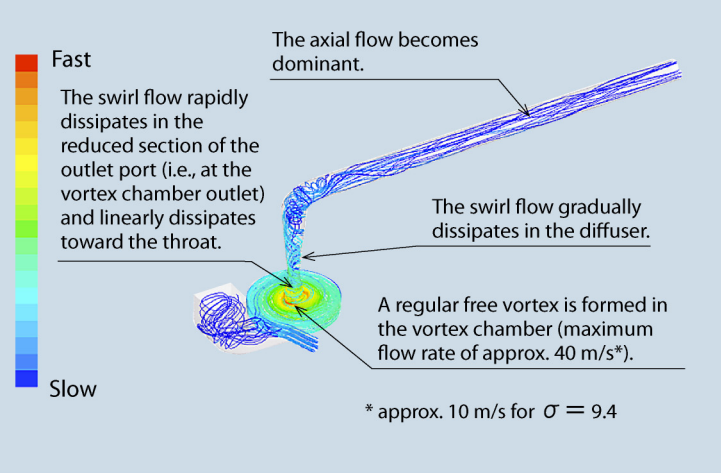

Figure 3 Flow pattern (σ = 0.3, 1/2-scale model)
The free vortex formed in the vortex chamber becomes a swirl flow with an axial component at the outlet pipe and quickly dissipates to become an axial flow.

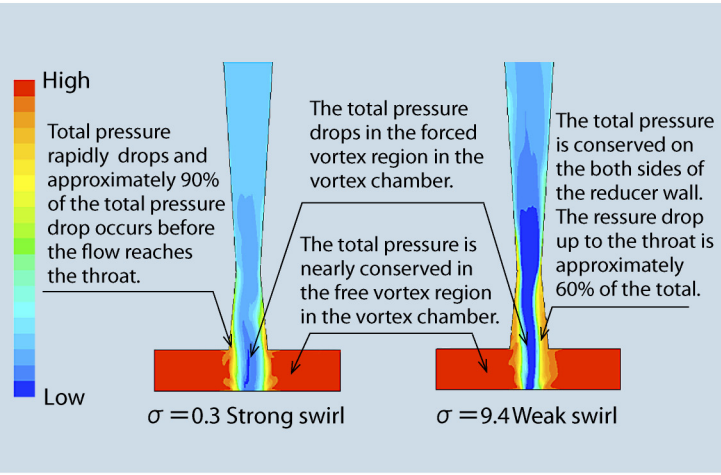

Figure 4 Total pressure distribution (scale = 1/5)
The total pressure drops in the forced vortex region at the center of the vortex chamber, and approx. 60% (σ = 9.4) to 90% (σ = 0.3) of the total pressure drop occurs up to the throat.

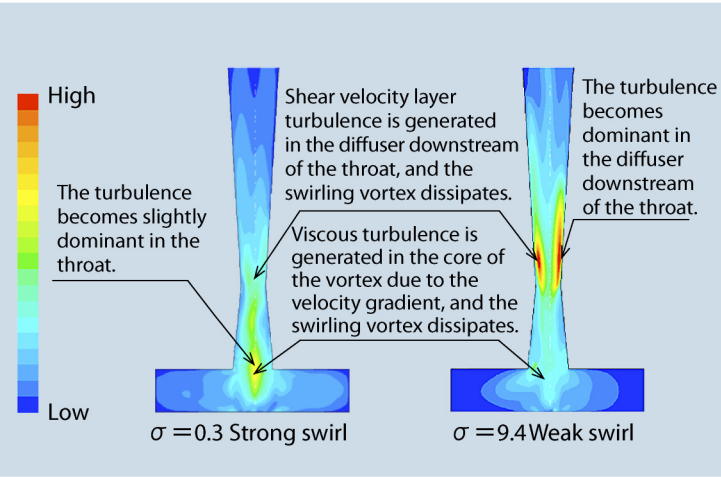

Figure 5 Turbulent energy distribution (scale = 1/5)
Turbulence is generated by the strong shear due to the viscosity in the vortex core. Turbulence is also generated in the shear velocity layer in the diffuser downstream of the throat.

- The formation of a regular free vortex in the vortex chamber accelerates the flow, and the static pressure is converted to dynamic pressure. The dynamic pressure increases toward the center of the vortex chamber.
- After leaving the vortex chamber, the regular vortex becomes a swirl flow with an axial component. This swirl flow quickly dissipates due to the generation of turbulence (strong shear due to the viscosity of the fluid) in the vortex core in the region between the center of the vortex chamber and the throat.

- After passing through the throat, the swirl flow dissipates due to the generation of turbulence in the shear velocity layer near the diffuser wall and eventually becomes a flow with only an axial component. Static pressure recovery becomes small in the diffuser downstream of the throat, resulting in a large pressure drop.
- Of the total pressure drop, 60% (σ = 9.4) to 90% (σ = 0.3) occurs in the region between the vortex chamber and the throat. Most of the remaining pressure drop takes place in the diffuser. The reason for this can be explained as follows. For σ = 0.3, when the swirl is strong, due to the large absolute value of the velocity gradient in the vortex core (the forced vortex region), the shear due to the viscosity of the fluid in the region between the center of the vortex chamber and the throat has a significant effect, resulting in a larger pressure drop along the path to the throat.

Figures 6–8 show the change in the cross section-averaged pressure and the turbulent energy at different locations. The pressure and turbulent energy were averaged over the concentric circular cross section of the vortex chamber and the cross section of the pipe downstream of the vortex chamber outlet. From these figures, the following conclusions can be drawn.

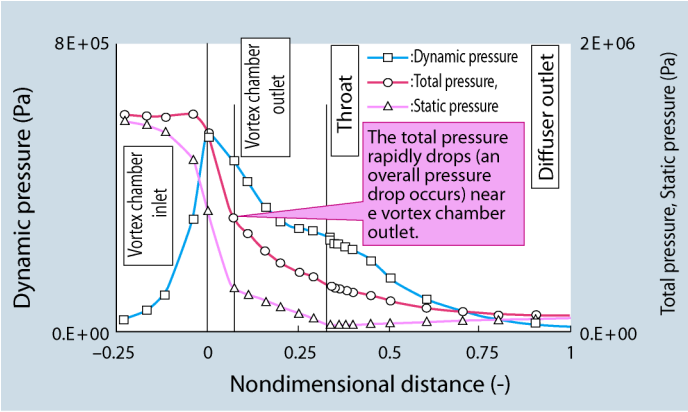

Figure 6 Cross section- averaged pressure distribution (σ = 0.3, 1/2-scale model)
The static pressure is converted to dynamic pressure in the free vortex region, and the total pressure drops rapidly near the vortex chamber outlet (an overall pressure drop occurs).

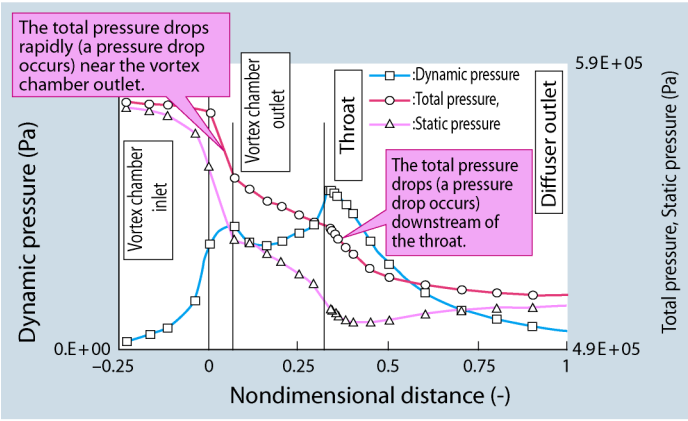

Figure 7 Cross section- averaged pressure distribution (σ = 9.4, 1/2-scale model)
Compared to σ = 0.3, the total pressure drops in two steps, and a large pressure drop occurs downstream of the throat.

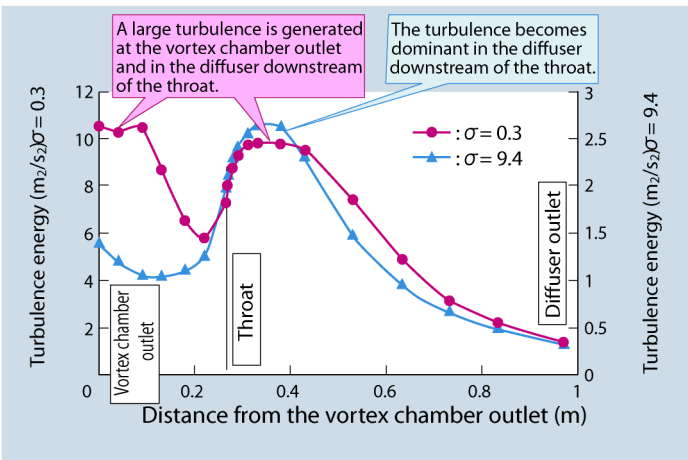

Figure 8 Change in cross section- averaged turbulent energy (1/2-scale model)
Turbulence is dominant at the vortex chamber outlet and downstream of the throat for σ = 0.3, and in the diffuser downstream of the throat for σ = 9.4.

- For σ = 0.3, the static pressure is converted to dynamic pressure in the free vortex region of the vortex chamber, and the dynamic pressure peaks near the vortex chamber outlet. The axial flow velocity increases near the throat, slightly increasing the dynamic pressure. The total pressure drops rapidly near the vortex chamber outlet, and thus an overall pressure drop occurs. The static pressure becomes the lowest at the throat and recovers slightly in the diffuser.
- For σ = 9.4, the static pressure in the vortex chamber is converted to dynamic pressure in the region toward the outlet, and the dynamic pressure increases once near the vortex chamber outlet. The axial flow velocity increases due to the reducer from the vortex chamber outlet to the throat. As a result, the dynamic pressure further increases, peaking at the throat. The total pressure rapidly drops near the vortex chamber outlet and downstream of the throat, and thus an overall pressure drop occurs. The static pressure becomes the lowest at the throat and recovers slightly in the diffuser.
- For σ = 0.3, when the swirl is strong, turbulence generation is strong in the region between the vortex chamber and the outlet nozzle, as well as in the diffuser downstream of the throat. For σ = 9.4, when the swirl is weak, turbulence generation is dominant in the diffuser downstream of the throat.

From the above discussion, the generation mechanism of the pressure drop appears to be the following.

- The formation of a regular free vortex in the vortex chamber accelerates the flow, causing the static pressure to be converted to dynamic pressure. The dynamic pressure increases toward the center of the vortex chamber.
- After leaving the vortex chamber, the regular vortex becomes a swirl flow with an axial component. This swirl flow quickly dissipates due to the generation of turbulence (viscous turbulence due to the velocity gradient) in the region between the center of the vortex chamber and the throat.
- After passing through the throat, the swirl flow quickly dissipates due to the generation of turbulence in the shear velocity layer near the diffuser wall and eventually becomes a flow with only an axial component.
- The above mechanism is independent of the cavitation number σ. For small values of σ, when the swirl is strong, due to the large absolute value of the velocity gradient in the vortex core (the forced vortex region), viscous turbulence caused by the velocity gradient in the region between the center of the vortex chamber and the throat has a significant effect, resulting in a larger pressure drop along the path to the throat.

Figure 9 compares the flow coefficient of the calculated and the experimental results.

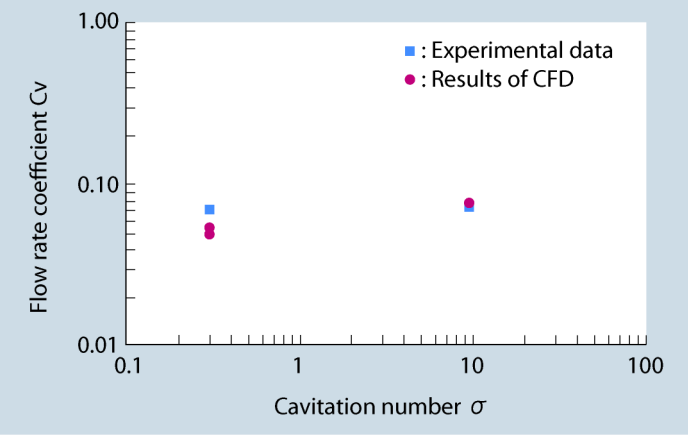

Figure 9 Calculated results of the flow coefficient (scale: 1/2)
The analysis accuracy is –25% for σ = 0.3 and +7% for σ = 9.4. It is slightly low for small values of σ, but generally agrees with the experimental results.

The analysis accuracy of the flow coefficient was –25% for σ = 0.3 and +7% for σ = 9.4. The accuracy was somewhat low for small values of σ, but agreed closely with the experimental results. The flow condition is thus similar to the experimental results. For σ = 0.3, the maximum and minimum values are plotted due to variations in the numerical solution. The reason for the slightly low flow coefficient for small values of σ can be explained as follows.

(1) The flow rate is higher for small values of σ, resulting in higher swirl intensity. A strong swirl makes the radial pressure gradient steeper due to centrifugal force. This may be the cause of the slightly low accuracy of the calculation in the turbulence model.

(2) The velocity is higher for small values of σ, resulting in y+ (the nondimensional distance between the wall and the first mesh point from the wall) approximately three times that for large values of σ. This may be the cause of the mesh dependence.

Figures 10 and **11** show the relationship between the calculated results of the flow coefficient and the model scales.

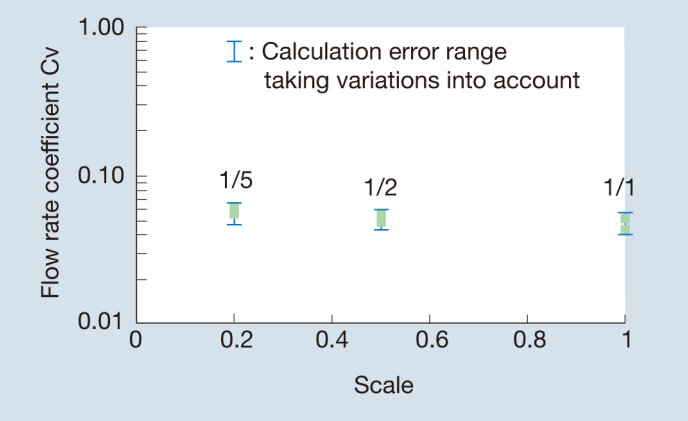

Figure 10 Comparison of the flow coefficients for σ = 0.3
The calculated flow coefficient is nearly constant for all scales within the range of calculation error for the variation of the solution specific to the vortex flow and mesh dependency.

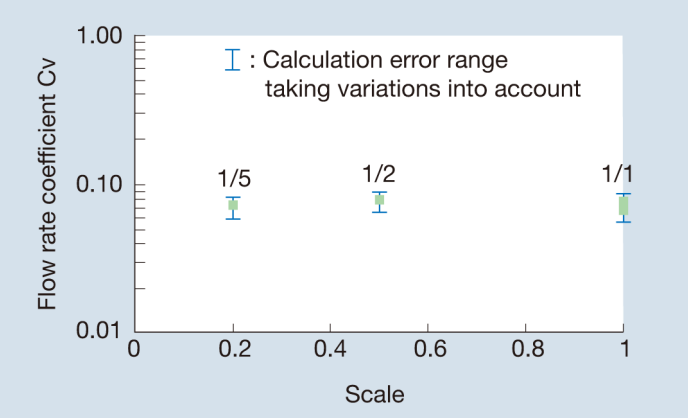

Figure 11 Comparison of the flow coefficients for σ = 9.4
The flow coefficient is nearly constant for all scales within the range of calculation error.

From these figures, the following conclusions can be drawn.

- The calculated flow coefficient is nearly constant for all scales within the range of calculation error.
- The possible contributors to calculation error are the mesh dependency (error: ±15%) and the error due to variations in the solution specific to the vortex flow (error: ±10% for σ = 0.3 and ±15% for σ = 9.4).

5. Conclusions

The flow condition in the advanced accumulator was investigated through CFD simulations. The turbulent behavior during small flow injection, which is difficult to assess experimentally, was evaluated numerically. The generation mechanism of pressure drop was also quantitatively investigated. The analysis predicted that the flow condition would be similar for all scales and that the flow coefficient for the actual accumulator would be comparable to that in the scale model experiment.

This investigation suggests that evaluation by numerical analysis complements experimental assessment and is effective in providing supporting evidence for the applicability of results of the scale-model experiment to a full-scale accumulator.

References

(1) Shiraishi et al., Development of Advanced Accumulator, Mitsubishi Heavy Industries Technical Review Vol. 31 No. 1 (1994) p. 14

(2) Shiraishi et al., "Jisedai PWR muke kokino akyumureta no kaihatsu (Development of Advanced Accumulator for the next-generation PWR) in Japanese," the journal of Thermal and Nuclear Power, Vol.45 No.6(1994).,

Authors

Tomoshige Takata
Manager
Takasago Research & Development Center, Technical Headquarters

Takafumi Ogino
Nuclear Energy Systems Engineering Center
Nuclear Energy Systems Headquarters

Takashi Ishibashi
Nuclear Energy Systems Engineering Center
Nuclear Energy Systems Headquarters

Tadashi Shiraishi
Special Adviser
MHI Nuclear Engineering Co., Ltd.